Comparison of the Structural Properties of the Active Site Cavities of Human and Rat Monoamine Oxidase A and B in Their Soluble and Membrane-Bound Forms†

Anup K. Upadhyay, Jin Wang, and Dale E. Edmondson*

Departments of Biochemistry and Chemistry, Emory University, Atlanta, Georgia 30322

Received October 1, 2007; Revised Manuscript Received November 13, 2007

ABSTRACT: Structural properties of the active site cavities in human and rat monoamine oxidases (MAOA and MAOB) have been studied in their detergent-purified and outer mitochondrial membrane (OMM) bound forms using a spin-labeled irreversible inhibitor (ParSL) as an active specific spin probe. ParSL has been found to be 5−10-fold more specific for human MAOB (hMAOB) with a K_i of ca. 20 μM, compared to K_i's in the range of 100−200 μM observed for other human and rat MAOs. Solvent accessibilities of the active-site-bound spin probes have been determined by studying the power saturation properties of the spin probe EPR signals in the presence and absence of a polar paramagnetic reagent NiEDDA and by measuring the extent of spin probe reductions on treatment with excess ascorbic acid. Results presented here show that the spin probe bound to the hMAOA active site is ca. 7−8-fold more accessible than in hMAOB. In contrast, the spin probes covalently attached to the two rat enzyme active sites show comparable accessibilities to each other. On comparison of human versus rat enzymes, the active-site-bound spin probes in the two rat MAOs show ca. 40% less accessibilities compared to the same in hMAOA but ca. 4−5-fold higher accessibilities than in hMAOB active site. The present data thus suggests that the structural properties of the active site cavities in rat MAOs are significantly different compared to those in the two human enzymes, which correlates with the differences reported earlier in the inhibitor specificities between human and rat MAOs.

Monoamine oxidases A and B (MAOA, MAOB[1]) are two outer mitochondrial membrane (OMM) bound enzymes involved in the oxidative degradation of monoamine neurotransmitters and xenobiotic amines. The three-dimensional structures of human MAOA (hMAOA), human MAOB (hMAOB), and rat MAOA (rMAOA) have been reported (*1*−*4*). The three enzymes show overall similarity in protein folds in their crystalline forms, as expected from their high sequence identities (∼70% between MAOA and MAOB and ∼90% between the homologous human and rat enzymes), but differ in oligomeric states and active site cavity structures. The enzymes bind to the outer mitochondrial membrane via C-terminal transmembrane helices with the entrances to their respective active sites thought to be located near the membrane surface (*5*, *6*). Both hMAOB and rMAOA crystallize as dimers, whereas hMAOA is a monomer in the crystal. The active site of hMAOB constitutes a dipartite cavity with a substrate entrance cavity (290 Å^3) connected to a larger substrate-binding cavity (420 Å^3) (*1*). Unlike hMAOB, the active sites in both rMAOA and hMAOA contain single substrate-binding cavities (i.e., no entrance cavities). The hMAOA cavity is larger (∼550 Å^3) than that in hMAOB (420 Å^3) or rMAOA (∼450 Å^3) (*3*, *4*). Consistent with the larger size of the substrate-binding cavity in hMAOA, the cavity shaping loop formed by residues 210−216 in hMAOA adopts an elongated conformation in the crystal structure compared to the same loop in hMAOB and rMAOA (*3*). No structural information is currently available for rMAOB.

A previous study on human and rat MAOA has shown differences in the mode of inhibitor binding and specificities of the two enzymes with the (*S*)-4-alkylthioamphetamine class of selective MAOA inhibitors (*7*). Similar differences in inhibitor specificities have also been reported between human and rat MAOBs (*8*). These observations raise doubts on the applicability of the rat enzymes in screening specific MAO inhibitors for clinical use in humans. On the basis of available structural information and docking studies, differences in kinetic properties between hMAOA and rMAOA have been attributed to the differences in the shapes and sizes of their active site cavities in the crystal structures (*7*). Due to the lack of structural information on rMAOB, origins of the observed differences in inhibitor specificities between human and rat MAOBs are not well understood. It should be noted, however, that previous kinetic studies on rMAOA and rMAOB are performed only with the mitochondrial membrane bound forms of the two enzymes (*7*, *8*). X-ray crystallographic structures of the detergent-purified MAOs may not reflect their physiological structures in the OMM-bound forms. Discrepancies in structural properties between crystallized and membrane-bound forms have been reported for many membrane proteins, e.g., bacterial vitamin B12

† This work was supported by National Institutes of Health Grant GM-29433 (D.E.E.).

* To whom correspondence should be addressed. E-mail: deedmon@emory.edu. Phone: 404-727-5972. Fax: 404-727-2738.

[1] Abbreviations: EPR, electron paramagnetic resonance; ParSL, spin-labeled pargyline analogue; MAO, monoamine oxidase; OGP, *n*-octyl-*β*-D-glucopyranoside; OMM, outer mitochondrial membrane; SDSL, site-directed spin labeling; mW, milliwatts; mT, millitesla (1 tesla = 10^4 gauss).

10.1021/bi7019707 CCC: $40.75
Published on Web 12/20/2007

transporter protein BtuB from *E. coli* (*9*, *10*). Our recent studies on the oligomeric states of human and rat MAOs in the OMM-bound and detergent-purified forms have shown that the monomeric X-ray structure observed for hMAOA is an effect of detergent purification. In the OMM-bound form, hMAOA is shown to remain as a dimer, like other human and rat MAOs (*11*). Although such alteration in oligomeric state on detergent purification is not uncommon for membrane proteins, and has also been reported for bovine mitochondrial ADP/ATP carrier (*12*−*14*), it may cause subtle variation in the active site structure, thereby altering its functional properties. Therefore, further studies using alternative spectroscopic approaches are needed to better understand the structural properties of the active site cavities of human and rat MAOs, in their detergent-purified as well as OMM-bound forms. This will allow the correlation of observed functional differences between human and rat MAOs with the structural differences in their active site cavities.

A widely used spectroscopic approach to understand the structural properties of soluble and membrane-bound proteins is the use of site-directed nitroxide spin labeling (SDSL) by cysteine-specific thiol reactive reagents and CW EPR spectroscopy (*15*−*23*). Several important structural aspects including dynamics of the protein conformation (*24*−*26*), polarity of the environment surrounding the spin probe (*15*, *27*, *28*), and solvent accessibilities of the protein surface and active sites (*29*−*34*) can be obtained using this method. Therefore, the SDSL-EPR technique can be used as a spectroscopic tool to compare the structural properties of membrane proteins in their detergent-purified or membrane-bound forms.

An alternative spin-labeling method by using spin-labeled inhibitors or substrate analogues as the active-site-specific spin probe for the target protein has also been reported in the literature for doing EPR spectroscopic studies in different contexts (*11*, *35*−*38*). Use of spin-labeled reversible and irreversible MAO inhibitors to probe the mechanism of substrate amine binding at the active sites using the CW EPR spectroscopic technique has been reported in previous studies (*38*−*40*). However, these previous studies were done at an early stage in our knowledge of the structural and functional properties of MAOs, and therefore no definitive information, regarding the differences in their active site architectures, could be obtained from these studies. In this work, we have used a spin-labeled pargyline analogue (ParSL), similar to those reported earlier (*38*), to study the variations in structural properties of different human and rat MAO active site cavities in their detergent-purified and OMM-bound forms. Accessibilities of the active-site-bound spin probes in human and rat MAOs to paramagnetic relaxation agent NiEDDA (*29*−*31*, *34*, *41*, *42*), or to the reducing agent ascorbic acid (*43*), have been determined. The results presented here provide useful insights into the species-dependent variations in structural properties of the MAO active site cavities, which correlate with the differences in inhibitor specificities reported earlier between human and rat MAOs (*7*, *8*).

EXPERIMENTAL PROCEDURES

Synthesis of Spin-Labeled MAO Inhibitor. The spin-labeled MAO inhibitor ParSL was synthesized by following the general method described earlier for the synthesis of a fluorescently labeled pargyline analogue, with minor modifications (*44*). Briefly, two mmol (458 mg) of *p*-bromomethyl phenyl acetic acid (Sigma) was dissolved in 25 mL of freshly distilled tetrahydrofuran (THF) in a 100 mL round-bottom flask and treated with 3 mL of thionyl chloride (Sigma). The mixture was refluxed for 1 h and evaporated to dryness. The dry residue was mixed with 200 mg of solid K_2CO_3 and 2 mmol (342 mg) of 4-amino tempo (Sigma) dissolved in 20 mL of dry THF. The mixture was left stirring at room temperature for 2 h and then refluxed for 30 min. The reaction mixture was cooled to room temperature, evaporated to dryness under reduced pressure, the residue was dissolved in 100 mL of chloroform, and the solution was washed five times with 0.5 N $NaHCO_3$, followed by two washings with distilled water to remove residual free acid and 4-amino tempo. The chloroform layer was dried over anhydrous sodium sulfate, filtered, and evaporated to dryness. The dried intermediate amide was immediately treated with 10 mL of freshly distilled ice-cold *N*-methyl propargylamine (Sigma) and stirred in the dark for 3 h at room temperature. The final product was then evaporated to dryness and dissolved in a minimum volume of chloroform. The chloroform layer was extracted with 20 mL volumes of 0.5 N HCl until the extract was colorless. All HCl extracts were combined, neutralized with solid K_2CO_3, and then re-extracted with three 50 mL volumes of chloroform. The combined chloroform extracts containing the crude product (ParSL) were dried over anhydrous sodium sulfate, evaporated to dryness, and further purified on a silica gel 60 (70−230 mesh, Merck) column using a stepwise increments of 25% (v/v) to 100% ethyl acetate−hexane solvent mixture. The purified product migrates with an $R_f = 0.29$ on silica gel 60 F_{254} TLC plates (Merck) using ethyl acetate as the solvent and shows a single mass peak with $m/z = 371.25$ ($M + 1H^+$). Nearly 200 mg of pure ParSL was obtained in a 25−30% yield.

Synthesis of NiEDDA. NiEDDA was synthesized using a previously reported method (*41*). Briefly, 5 mmol (881 mg) of ethylenediamine-*N*,*N*′-diacetic acid (EDDA, Sigma) was dissolved in 300−400 mL of distilled water in a 1 L round-bottom flask and stirred until completely dissolved. To this solution, 5 mmol of (464 mg) $Ni(OH)_2$ (Sigma) was added, and the turbid green solution was heated to 50−60 °C until all the insoluble green $Ni(OH)_2$ was converted to the soluble, blue NiEDDA. The solution was left stirring for an additional 18 h at 20−22 °C and then filtered to remove any residual particulate material. Water was removed under vacuum, and the solid residue was washed with methanol to remove any remaining $Ni(OH)_2$ or EDDA. The final product was dried under vacuum and characterized by ESI-MS (*m*/*z* peak at 231 Da).

Expression and Purification of Human and Rat MAOs. Recombinant human hMAOA and hMAOB were expressed and purified from a *Pichia pastoris* expression system as described previously (*45*, *46*). Expression and purification of recombinant rMAOA and rMAOB were done following a procedure to be reported elsewhere. Briefly, cDNAs for rat MAOA and rat MAOB were cloned from a rat liver cDNA library and expressed in *P. pastoris* following general procedures published for the human enzymes (*45*, *46*). Purification of the rat enzymes in *n*-octyl-β-D-glucopyranoside (OGP) detergent micelles (Sigma) was done following similar protocols as with the human enzymes with minor

adjustments in pH and salt concentrations during the purification procedures (*45*−*47*).

Preparation of OMM. Outer mitochondrial membranes were isolated following a previously reported method (*48*). *P. pastoris* mitochondria were isolated by enzymatic disruption of the yeast cell wall using the spheroplasting method followed by sequential centrifugation. The intact mitochondria were disrupted by osmotic shock and sonicated to liberate the OMM. OMM were isolated on a 30−55% (w/v) sucrose density gradient at 20 000 rpm (Beckman SW-28 rotor) for 15 h. The OMM fraction formed a separate band near 40−45% (w/v) density of sucrose, which contained all of the MAO activity. This layer was diluted with three volumes of 10 mM Tris−HCl buffer, pH 7.4, and pelleted by a 1 h centrifugation at 35 000 rpm using a Beckman Ti-45 rotor. The OMM pellets were suspended in 50 mM potassium phosphate buffer at pH 7.4 containing 10% (v/v) glycerol and kept frozen in small aliquots at −80 °C until used.

UV−*Vis Spectroscopic Studies and Enzyme Activity Assays.* UV−vis spectra were recorded on a Varian Cary-50 UV−vis spectrophotometer. Enzyme activities of OMM-bound and detergent-purified human and rat MAOs were measured optically by monitoring the rate of product formation over time using a Perkin-Elmer Lambda 2 spectrophotometer. Activities of human and rat MAOAs were measured by monitoring the oxidation of kynuramine at 316 nm. The activities of human and rat MAOBs were followed at 250 nm using benzylamine as substrate. All enzyme assays were done in 50 mM HEPES buffer at pH 7.5. For detergent-purified samples the activity buffer also contained 0.5% (w/v) reduced Triton X-100 (*47, 49*).

Measurements of Inhibition Constants of ParSL for OMM-Bound Human and Rat MAOs. Inhibition constants of ParSL for the OMM-bound human and rat MAOs were determined by measuring the kinetic parameters in the presence of 3−5 different concentrations of ParSL in the activity buffer. The apparent K_m values for benzylamine (human and rat MAOBs) or kynuramine (human and rat MAOAs) with different concentrations of ParSL inhibitor were determined using Lineweaver−Burk plots and plotted versus ParSL concentrations to calculate the K_i values using the standard kinetic equation for competitive inhibition.

Preparation of ParSL-Labeled OMM-Bound MAO Samples. The ParSL-labeled OMM-bound MAO samples were prepared by adding ca. 50-fold molar excess of ParSL to the samples and incubating at room temperature on a rotating wheel at 10−20 rpm. Concentrations of MAOs in the OMM suspensions were estimated by comparing the units of activity per milliliter of membrane suspension with that of the corresponding purified enzymes of known concentrations. The extent of inhibitor binding at the active sites was monitored by measuring the loss of activity with time. Usually it required ca. 10−20 min of incubation for complete inhibition of the human MAOB samples and nearly 40−60 min of incubation for all other human and rat MAOs. No nonspecific loss of activity was observed in the control OMM samples incubated under similar conditions. For the EPR studies on ParSL-inhibited OMM samples, excess inhibitor was removed by three cycles of 1 h centrifugation at 100 000*g* and resuspension in 60 mL of 50 mM potassium phosphate (KPi) buffer pH 7.4. The final pellets were suspended in small volume (usually ca. 100−200 μL) of 50 mM KPi buffer containing 10% (v/v) glycerol, pH 7.4, and stored at −80 °C until EPR measurements.

Preparation of ParSL-Labeled Detergent-Purified Samples. Detergent (OGP) purified ParSL-inhibited MAO samples were labeled by adding 50-fold excess of the inhibitor (ParSL) and incubating at room temperature on a rotating wheel as for the OMM samples mentioned above. The extent of ParSL binding at the MAO active sites were determined by measuring the loss of enzyme activities with time and by optically monitoring the concomitant formation of flavocyanine adducts (absorption maxima near 400−410 nm). For hMAOB samples, 90−100% inhibition was observed within 1 h of incubation at room temperature. Complete inhibitions of all other MAOs required 3−4 h of incubation. The control samples incubated under similar conditions showed no loss of activity. The detergent-purified EPR samples of the ParSL-inhibited proteins were prepared by removing the excess ParSL by ion exchange chromatography using a Bio-Rad MacroPrep High-Q column (Bio Rad Laboratories, Hercules, CA) for MAOBs or DEAE Sepharose Fast Flow (Amersham Biosciences, Uppsala, Sweden) column for MAOAs. The columns were pre-equilibrated with 10 mM KPi, 20% glycerol, 0.8% OGP pH 7.4 (buffer A) before loading the ParSL-inhibited samples. The columns were then washed with 20 column volumes of buffer A. Elution of the ParSL-labeled MAO from the column was done using buffer containing 200 mM KPi, 20% (v/v) glycerol, 0.8% (w/v) OGP, adjusted to pH 7.4. The elution buffer was exchanged by two washings with 50 mM KPi, 20% (v/v) glycerol, 1.2% (w/v) OGP, pH 7.4 using Millipore molecular weight cutoff filters. The samples were concentrated to nearly 50−60 μM protein (spin label) concentration.

CW EPR Spectroscopic Study. X-band (9.4 GHz) CW EPR spectra were recorded on a Bruker 200D instrument equipped with a Bruker ST4102/8216 TE102 cavity. Microwave frequency was measured with a HP 4256L frequency counter. Temperature was regulated by using a modified Air Products cryostat and temperature controller with nitrogen gas flow system. All spectra were recorded at 25 °C with 100 kHz modulation frequency and 2 G modulation amplitude, unless mentioned otherwise. Samples were loaded in quartz capillaries of 1.0 mm i.d. and 2.0 o.d. and placed in a regular X-band EPR sample tube of 3 mm i.d. and 4 mm o.d. Spin quantitations were performed using SpinCount software, developed by Dr. Michael P. Hendrich (Carnegie Mellon University, Pittsburgh, PA), by comparing the double integrals of the EPR spectra recorded on the ParSL-inhibited MAO samples with that of a freshly prepared potassium nitrosodisulfonate (Sigma) spin standard of known concentration ($\epsilon_{545} = 20.8\ M^{-1}\ cm^{-1}$) (*50*).

Measurements of Accessibilities of the Spin Label to NiEDDA. Accessibility of the active-site-bound ParSL spin probe to the paramagnetic reagent (NiEDDA) was determined by doing power saturation CW EPR studies (*29, 31, 41, 51*) with incident microwave powers ranging from 0.2 to 63 mW. The experiments were performed under air saturation with the reasonable assumption that the collisional spin relaxation due to molecular oxygen is similar between samples with and without NiEDDA (*29*). The power saturation curves were drawn by plotting the peak-to-peak (p−p) amplitudes (A) of the central $M_I = 0$ line of the first

derivative nitroxide spectrum versus the incident microwave powers (P). Since the intensities of the EPR signals varied between samples depending on spin concentrations, p−p intensities of the $M_I = 0$ lines recorded at the lowest microwave power (unsaturated intensity) for all samples were scaled to unity. The intensities ($M_I = 0$ lines) of all other spectra, recorded at increasing incident microwave powers, were scaled using the respective scaling factor for each sample. This allowed us to visualize power saturation curves for multiple samples in the same graph (Figures 4 and 5) with a uniform Y-scale. The resulting curves were fit to eq 1 using Origin 6.0:

$$A = IP^{1/2}[1 + (2^{1/\epsilon} - 1)P/P_{1/2}]^{-\epsilon} \quad (1)$$

where I is a scaling factor, $P_{1/2}$ is the power required to reduce the amplitude of the $M_I = 0$ line to half of its unsaturated value, and ϵ is a measure of the homogeneity of saturation of the resonance line. The value of ϵ ranges between 1.5 and 0.5 for homogeneous and inhomogeneous saturation limits, respectively (*29*, *31*, *41*). For the simulations shown in this work, the parameters I and $P_{1/2}$ were allowed to vary freely, while ϵ was varied between 0.5 and 1.5 (*29*, *52*).

The parameter $\Delta P_{1/2}$, measuring the difference between $P_{1/2}$ values in the presence ($P_{1/2}$) and in the absence ($P_{1/2}{}^0$) of 5 mM NiEDDA was calculated from the fits. The collision frequency (W) of the spin label with the paramagnetic relaxation agent (NiEDDA) is proportional to $\Delta P_{1/2}$ divided by p−p width of the $M_I = 0$ line (ΔH_0), as shown below in eq 2 (*29*, *31*, *41*):

$$W = \frac{\Delta P_{1/2}}{\Delta H_0} \quad (2)$$

Relative accessibility (R_a) of the spin probe between two samples is compared by taking the ratio of the collision frequencies (W) for different samples. Since EPR spectra recorded for all samples showed comparable p−p width of the $M_I = 0$ line (ΔH_0) of ∼8 G, R_a values could be calculated by directly taking the ratios of the $\Delta P_{1/2}$ values for the two different samples (eq 3).

$$R_a = \frac{(\Delta P_{1/2})_{\text{sample1}}}{(\Delta P_{1/2})_{\text{sample2}}} \quad (3)$$

Measurement of Spin Probe Accessibility by Reduction with Ascorbic Acid. Accessibilities of the spin probes were also measured by monitoring the extent of reduction of the spin probe with 3 mM ascorbic acid (*43*). The spin-labeled detergent-purified samples were treated with 3 mM (final concentration in the sample) ascorbic acid and incubated at room temperature. EPR spectra were recorded after 10 and 20 min of incubation. The EPR spectral intensities were compared before and after ascorbic acid treatments to determine the extent of spin probe reductions.

Superposition of ParSL in the hMAOA and hMAOB Active Sites. The ParSL superimposed structures of hMAOA and hMAOB were generated using program O version 7.0.1 (*53*). The energy-minimized coordinates of different rotamers of the ParSL molecule were generated by CS Chem3D Pro 5.0 (Cambridge Soft. Corp.) software and saved as PDB files.

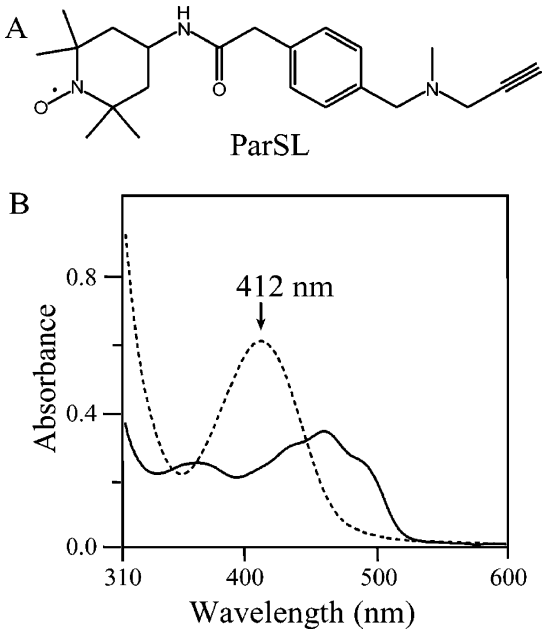

FIGURE 1: (A) Structure of spin-labeled MAO inhibitor used in this work. (B) Optical spectra of the native (solid line) and ParSL-inhibited (dashed line) hMAOA. The arrow indicates the absorption maxima (410 nm) of the hMAOA−ParSL N5−flavocyanine adduct.

Table 1: Competitive Inhibition Constants (K_i's) of ParSL for OMM-Bound Human and Rat MAOs

enzyme	K_i (μM) (av ± SD)
hMAOB	22 ± 5
hMAOA	212 ± 22
rMAOB	107 ± 21
rMAOA	151 ± 49

The optimized ParSL rotamers were manually superimposed with the original inhibitor molecules (Clorgyline in hMAOA, Pargyline in hMAOB) present in the X-ray structures of hMAOA (PDB ID: 2BXS) and hMAOB (PDB ID: 1GOS). The orientation of the ParSL inhibitor was adjusted as required to minimize the side chain interactions and to maximize the overlap with the existing inhibitor. The superimposed structures were visualized using PyMol v.99 molecular graphics software (http://www.pymol.org).

RESULTS

Inhibition of Human and Rat MAOs with ParSL. The structure of the pargyline-based spin-labeled MAO inhibitor (ParSL) used in this work is shown in Figure 1A. Like other *N*-methylpropargylamine-based irreversible inhibitors (e.g., pargyline, clorgyline), ParSL inhibits all human and rat MAOs reversibly in a competitive manner prior to forming covalent N5−flavocyanine adducts (*45*, *46*). The inhibition constants (K_i's) of ParSL are measured for the OMM-bound human and rat MAOs and are listed in Table 1. As evident from Table 1, ParSL is ca. 5−10-fold better inhibitor for hMAOB compared to all other human and rat MAOs. The large difference in K_i values of ParSL between human and rat MAOBs is consistent with the differences in inhibitor specificities reported between them in a previous study (*8*). In order to compare the efficacy of ParSL as an irreversible MAO inhibitor relative to pargyline, limiting rates of inactivation of OMM-bound hMAOB by ParSL and by pargyline have been determined from Kitz−Wilson plots (not

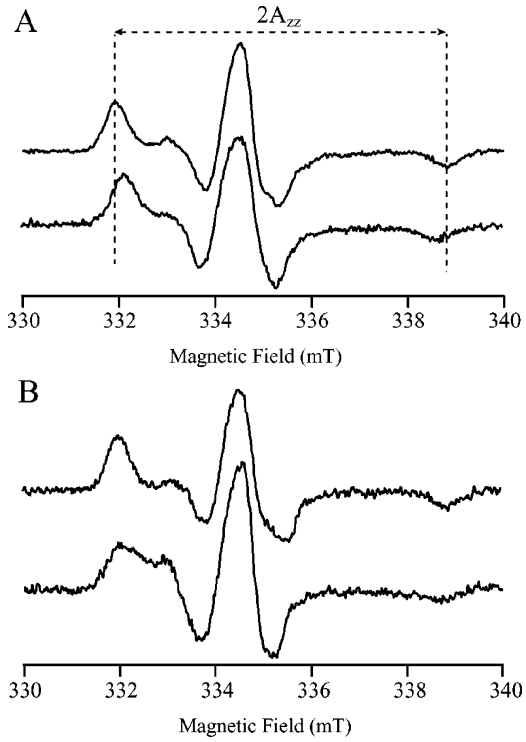

FIGURE 2: X-band (9.4 GHz) EPR spectra of the ParSL-inhibited, detergent-purified (upper traces) and OMM-bound (lower traces) MAO samples of (A) hMAOA and (B) rMAOA. Instrument parameters: microwave power 2.0 mW, modulation amplitude 2 G, modulation frequency 100 kHz, temperature 298 K.

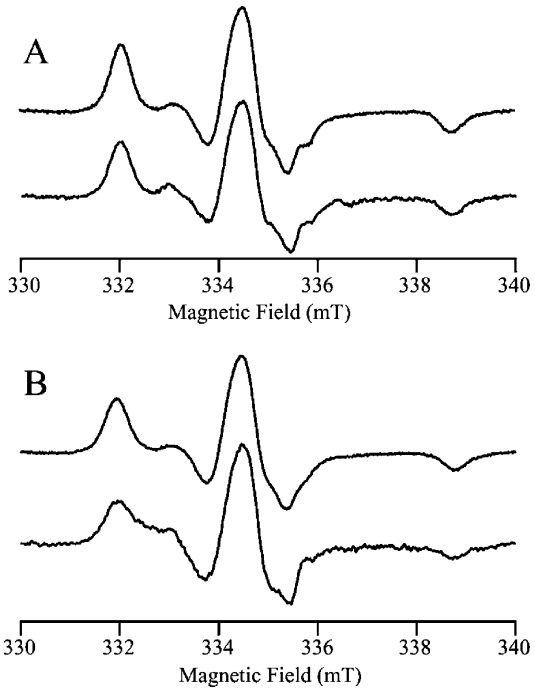

FIGURE 3: X-band (9.4 GHz) EPR spectra of the ParSL-inhibited, detergent-purified (upper traces) and OMM-bound (lower traces) MAO samples of (A) hMAOB and (B) rMAOB. Instrument parameters are the same as listed in the caption of Figure 2.

shown) (*54*, *55*). The rates of inactivation are found to be 0.11 min^{-1} with ParSL as compared to a rate of 0.43 min^{-1} with pargyline. These data demonstrate that the covalent flavocyanine adduct formation between OMM-bound hMAOB and ParSL is ca. 4-fold slower than that of pargyline. The formation of flavocyanine adducts on inhibition with ParSL could be monitored for the detergent-purified samples from the characteristic changes in the UV−vis absorption spectrum. Optical spectra recorded on detergent-purified native (solid line) and ParSL-inhibited (dashed line) hMAOA samples are shown in Figure 1B. The arrow at 412 nm (Figure 1B) indicates the absorption maxima of the N5−flavocyanine adduct. Inhibition of all other human and rat MAOs with ParSL showed appearances of a similar peak near 400−410 nm, demonstrating the formation of N(5)−flavocyanine adduct for each MAO sample (not shown). These spectral and kinetic data demonstrate the applicability of ParSL as an active-site-specific covalent spin probe for all human and rat MAOs, in studying their structural properties in detergent-purified and OMM-bound forms using the EPR spectroscopic technique (vide infra).

CW EPR Measurements. Room-temperature X-band (9.4 GHz) EPR spectra recorded on the ParSL-inhibited detergent-purified and OMM-bound human and rat MAOA samples are shown in Figure 2, parts A and B, respectively. The EPR spectra recorded on the corresponding human and rat MAOB samples are shown in Figure 3, parts A and B, respectively. The EPR spectra of the detergent-purified samples are shown in the upper traces and those of the OMM-bound samples are shown in the lower traces of the two panels in Figures 2 and 3. As evident from the spectral line shapes, spin probes in all samples (Figures 2 and 3) are in the slow motional regime (*15*, *29*, *56*), indicating that the ParSL inhibitors are rigidly bound to the MAO active sites with limited mobility in the X-band EPR time scale.

The separation between the two outermost peaks ($2A_{zz}$) is ca. 0.4 mT smaller in the EPR spectrum of the OMM-bound hMAOA sample, compared to its detergent-purified form (dashed vertical lines in Figure 2A). Spectra recorded at low temperature (120 K) on these samples also show a similar difference in $2A_{zz}$ values (not shown), indicating that the polarity of the environment surrounding the nitroxide spin probe in the hMAOA active site becomes more polar on detergent extraction from the membrane (*15*, *28*, *57*). This may originate from subtle alterations in the protein conformation in OGP (detergent) micelles relative to the membrane-bound form. EPR spectra recorded on other human and rat MAOs do not show any significant differences in $2A_{zz}$ values between their OMM-bound and detergent (OGP) purified forms. Therefore, the current EPR data suggests that the conformation of hMAOA is more sensitive to purification in OGP micelles compared to other human and rat MAOs. This data agrees with previous studies showing lower stability and higher conformational flexibility of hMAOA compared to hMAOB in detergent micelles (*58*). Spin quantitations of the EPR signals from the detergent-purified samples agree (within error) with the expected 1:1 protein to nitroxide stoichiometry.

Accessibility Measurements Using NiEDDA. Solvent accessibilities of the active-site-bound ParSL spin probes were determined by measuring the power saturation properties of the nitroxide EPR signals with the paramagnetic reagent NiEDDA (*29*, *31*, *41*, *51*). The incident microwave power was varied from 0.2 to 63 mW. The power saturation curves were obtained by plotting the normalized (cf., Experimental Procedures) peak-to-peak amplitudes of the central $M_I = 0$ lines of ParSL-inhibited detergent-purified and OMM-bound human and rat MAO samples in the presence and in the

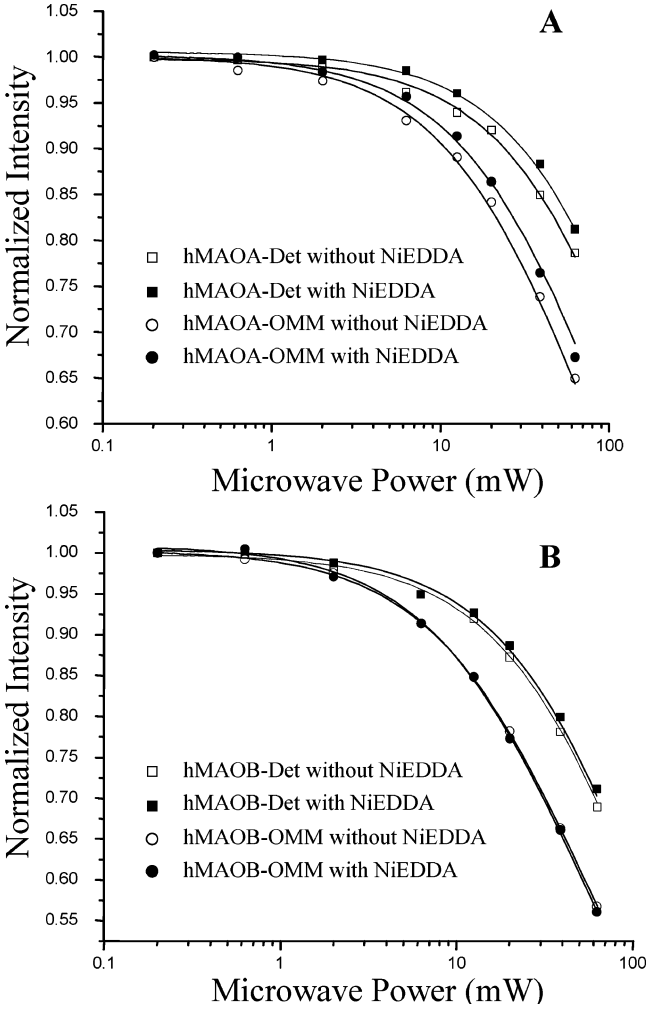

FIGURE 4: Power saturation study on ParSL-inhibited (A) detergent-purified (squares) and OMM-bound (circles) hMAOA in the presence (filled symbols) and in the absence (empty symbols) of 5 mM NiEDDA. (B) Detergent-purified (squares) and OMM-bound (circles) hMAOB in the presence (filled symbols) and absence (empty symbols) of 5 mM NiEDDA. The solid lines in the figure are fits to the data obtained using eq 1 (cf., Experiment Procedures). Individual data sets are identified in the figure insets. All EPR spectra were recorded with 2 G modulation amplitude and 100 kHz modulation frequency at 25 °C. The microwave power varied from 0.2 to 63 mW. Microwave frequency was 9.4 GHz.

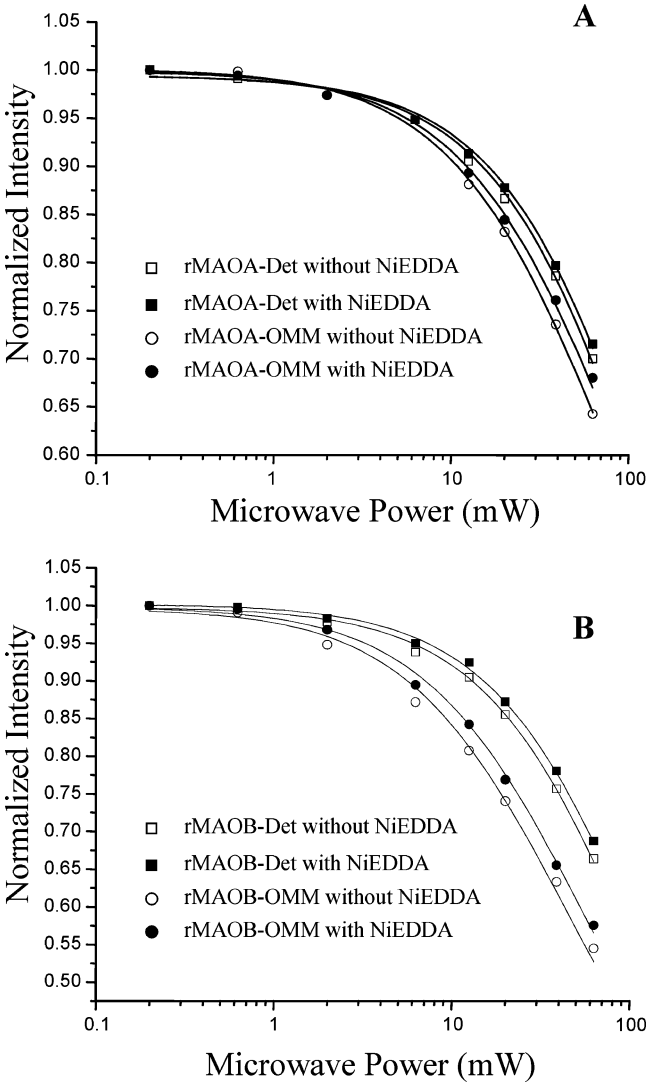

FIGURE 5: Power saturation study on ParSL-inhibited (A) detergent-purified (squares) and OMM-bound (circles) rMAOA samples in the presence (filled symbols) and in the absence (empty symbols) of 5 mM NiEDDA. (B) Detergent-purified (squares) and OMM-bound (circles) rMAOB in the presence (filled symbols) and absence (empty symbols) of 5 mM NiEDDA. The solid lines in the figure are fits to the data obtained using eq 1 (cf., Experiment Procedures). Individual data sets are identified in the figure insets. Instruments settings used are mentioned in Figure 4.

absence of 5 mM NiEDDA. The power saturation data obtained on the hMAOA and hMAOB samples are shown in Figure 4, parts A and B, respectively. Corresponding power saturation data for rMAOA and rMAOB samples are shown in Figure 5, parts A and B. The lines drawn through the data points in the Figures 4 and 5 are fits to the data obtained using eq 1 (cf., Experimental Procedures). The power required in attaining half-saturation ($P_{1/2}$) of the EPR signal intensities in the presence and the absence of NiEDDA are obtained from the fits and used in calculating $\Delta P_{1/2}$ values (Table 2). The relative accessibilities (R_a) of the ParSL spin probes, covalently bound to human and rat MAO active sites, are calculated based on eq 3 (cf., Experimental Procedures) and summarized in Table 3.

The relative accessibility values listed in Table 3 show that the spin probe in the hMAOA active site is ca. 7−8-fold more accessible than the same in hMAOB, in both detergent-purified and OMM-bound forms. This is in agreement with the crystallographic data showing a less elongated and wider active site cavity in hMAOA (4). In contrast to human MAOs, the active site cavities in the two rat enzymes

Table 2: Differences (Average ± SD) in Power at Half-Saturation ($\Delta P_{1/2} = P_{1/2} - P_{1/2}^0$) in the Presence ($P_{1/2}$) and Absence ($P_{1/2}^0$) of NiEDDA Obtained for All ParSL-Inhibited Human and Rat MAO Samples from the Fits Shown in Figures 4 and 5[a]

sample	$\Delta P_{1/2}$ (mW)
hMAOA-$_{Det}$	20 ± 3
hMAOA-$_{OMM}$	33 ± 5
rMAOA-$_{Det}$	13 ± 2
rMAOA-$_{OMM}$	20 ± 2
hMAOB-$_{Det}$	3 ± 1
hMAOB-$_{OMM}$	4 ± 1
rMAOB-$_{Det}$	14 ± 3
rMAOB-$_{OMM}$	17 ± 2

[a] Subscripts "Det" represent detergent-purified form and "OMM" represent outer mitochondrial membrane bound form of the respective enzyme.

Table 3: Summary of Relative Solvent Accessibilities (R_a) of Human and Rat MAOs Calculated Based on Eq 3 and the $\Delta P_{1/2}$ Values in Table 2[a]

		R_a (av ± SD)
MAOA vs MAOB in the detergent and in the OMM	$(hMAOA)_{Det}/(hMAOB)_{Det}$	7.2 ± 2.4
	$(hMAOA)_{OMM}/(hMAOB)_{OMM}$	8.2 ± 2.5
	$(rMAOA)_{Det}/(rMAOB)_{Det}$	0.96 ± 0.23
	$(rMAOA)_{OMM}/(rMAOB)_{OMM}$	1.19 ± 0.16
human vs rat MAOs	$(rMAOA)_{Det}/(hMAOA)_{Det}$	0.66 ± 0.12
	$(rMAOA)_{OMM}/(hMAOA)_{OMM}$	0.61 ± 0.1
	$(rMAOB)_{Det}/(hMAOB)_{Det}$	5 ± 1.8
	$(rMAOB)_{OMM}/(hMAOB)_{OMM}$	4.4 ± 1.1

[a] Subscripts "Det" and "OMM" represent detergent-purified and outer mitochondrial membrane bound form, respectively, for the respective enzyme.

show comparable solvent accessibilities to each other in their detergent-purified and OMM-bound forms (Figure 5, Table 3). These results suggest that the structural properties of the active site cavities in the two rat MAOs are similar, whereas the two human enzymes have distinctly different active site structures.

Comparison between human and rat MAOs shows that the active site cavities in the two rat enzymes are nearly 40−50% less accessible compared to hMAOA but nearly 4−5-fold more accessible than that in hMAOB (Table 3). Relative solvent accessibilities of the active-site-bound ParSL spin probes in human and rat MAOs can be arranged in a decreasing order as follows: hMAOA > rMAOA ≈ rMAOB > hMAOB. This trend is similar in both detergent-purified and OMM-bound forms, which indicates that the overall structural properties of the active site cavities in human and rat MAOs remain similar in their OMM-bound and detergent-purified forms.

Accessibility Studies of the MAO Active-Site-Bound ParSL Spin Probes Studied by Ascorbic Acid Reduction. To further investigate the differences in accessibility of the human and rat MAO active site cavities, EPR spectra were recorded on the ParSL-inhibited detergent-purified samples before (solid lines) and after (dashed lines) treatment with excess (3 mM) ascorbic acid (Figure 6). If the active-site-bound spin probe is more accessible to solvent, it will undergo more reduction on treatment with ascorbic acid under similar conditions, as compared to a less accessible spin probe.

Consistent with the NiEDDA data shown above (Figures 4 and 5), the highest accessibility of the active-site-bound spin probe was observed in the hMAOA sample (Figure 6A) showing ca. 90% reduction of the spin probe EPR signals within 10 min of incubation with 3 mM ascorbic acid at room temperature. The spin probe bound to the hMAOB active site cavity is found to be least accessible, undergoing only 10% reduction after 20 min of incubation with 3 mM ascorbic acid (Figure 6B). Similar incubations of the ParSL-inhibited rMAOA and rMAOB samples for 20 min with 3 mM ascorbic acid show 50% and 30% reductions, respectively (Figure 6, parts C and D, respectively).

A similar trend in ascorbic acid reductions of the active-site-bound spin probes has also been observed for OMM-bound hMAOA and hMAOB samples (not shown). However, the OMM-bound samples, incubated under similar conditions as the corresponding detergent-purified samples, show much lower levels of reduction of the spin probes. On the basis of X-ray structural studies, it has been suggested that the entrance to the MAO active site is located near the membrane

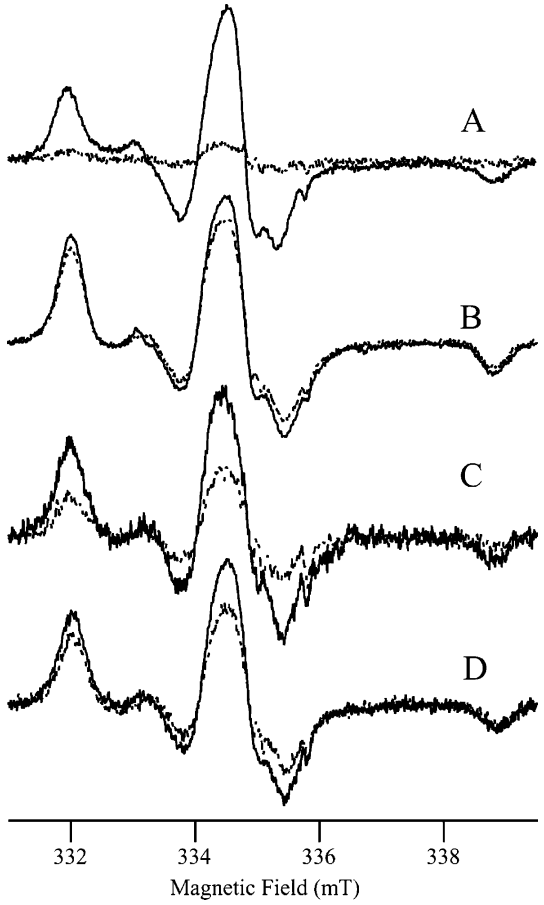

FIGURE 6: EPR spectra recorded on oxidized (solid lines) and ascorbic acid treated (dashed lines) samples of ParSL-inhibited human and rat MAOs in their detergent-purified forms: (A) hMAOA, (B) hMAOB, (C) rMAOA, (D) rMAOB. Instrument parameters are the same as listed in the caption of Figure 2.

surface (*1*, *6*). Therefore, the repulsive interactions between the negatively charged phosphate head groups of the lipids at the surface of the OMM and negatively charged ascorbic acid anion at pH 7.4 could hinder access to the active-site-bound spin probe, thereby reducing the observed levels of spin probe reduction. NiEDDA, being neutral (*41*), does not encounter such an electrostatic repulsion and can access the spin probe, unless buried inside the protein active site.

DISCUSSION

The results presented above elucidate the variations in structural properties of the active site cavities in human and rat MAOs, which correlate to their differences in inhibitor

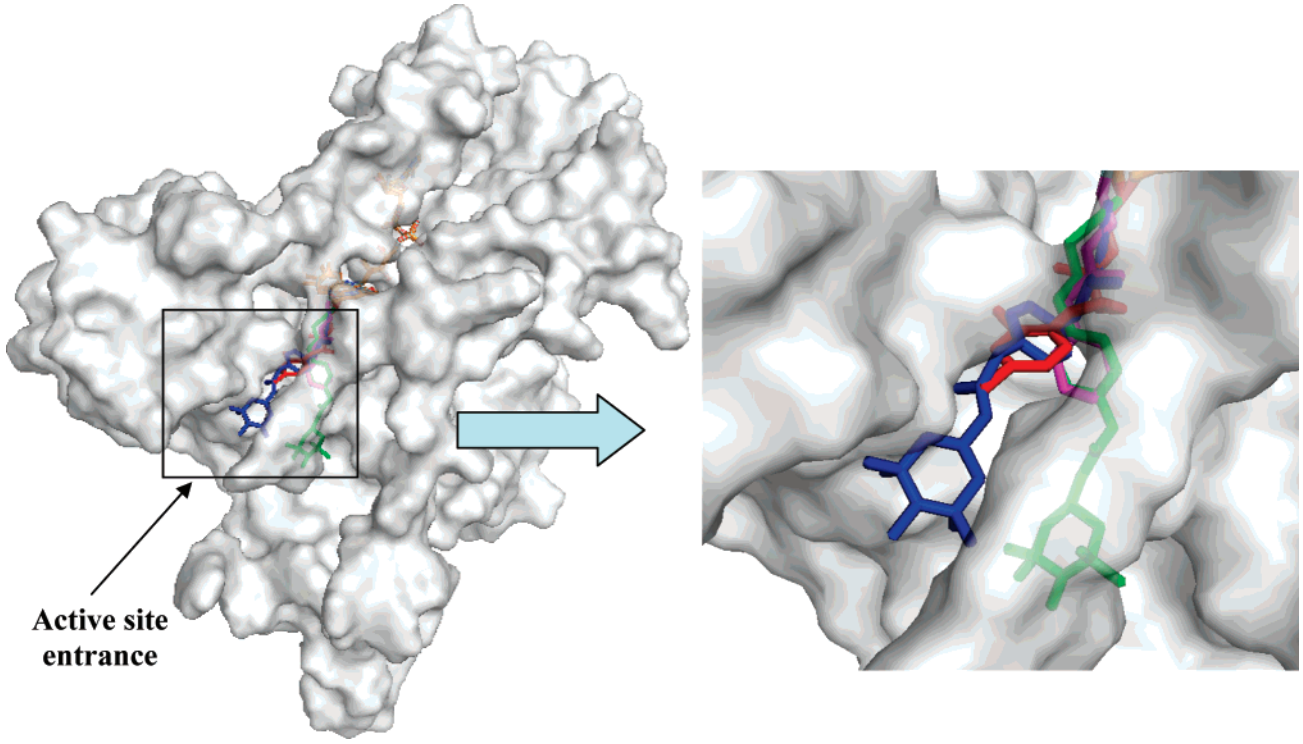

FIGURE 7: Aligned structures of clorgyline-inhibited hMAOA (PDB ID: 2BXS) and pargyline-inhibited hMAOB (PDB ID: 1GOS) with ParSL inhibitor superimposed on the original inhibitors in their respective active sites. Only one subunit of the hMAOB structure is shown. Clorgyline in the hMAOA structure is shown in red and pargyline in the hMAOB structure is shown in magenta. The ParSL molecule superimposed in the hMAOA structure is shown in blue, and the ParSL molecule superimposed in the hMAOB structure is shown in green. The superimposed structures of the inhibitors are displayed within a translucent molecular surface representation of hMAOA. The figure is rendered using PyMol v.99 software (http://www.pymol.org).

specificities reported in previous studies (*7*, *8*). The *P. pastoris* expression system and the uniform purification protocol used in this study eliminates the possibility of observing artifactual structural and functional differences due to variations in membrane lipid compositions or the choice of detergent micelle used for protein purifications. The major spectroscopic observations and their possible significances are discussed below in the light of available knowledge on structural and functional properties of human and rat MAOs.

Structures of MAO Active Site Cavities in OMM-Bound and Detergent-Purified Forms. Structural properties of membrane proteins are known to depend on the choice of detergent micelles used in purification or reconstitutions (*59*). Therefore, one of the major challenges in structural and functional studies on membrane proteins is to ascertain that their properties do not change significantly on purification in detergent micelles. Our recent studies have shown that the dimeric structures of human and rat MAOAs in the OMM partially dissociate to monomeric forms on purification in OGP micelles, which has been attributed as a reason for the monomeric X-ray structure of hMAOA (*3*, *11*). Although the overall protein folds observed for hMAOA in its monomeric crystal structure are similar to those in the dimeric crystal structures of hMAOB and rMAOA (*1*, *3*, *4*), alteration in oligomeric state can affect its active site architecture. Furthermore, available X-ray structural data on hMAOA (OGP), rMAOA (*N*-dodecylphosphocholine), and hMAOB (Zwittergent 3-12) were obtained from crystals grown in different detergent micelles with varying miceller properties, which can potentially cause the subtle differences observed in their structures. The present structure−function correlation study on human and rat MAOs, using uniform miceller and membrane environments, was thus imperative in explaining the differences in their functional properties (*7*, *8*).

As evident from the results presented above (Table 3), the relative accessibility of the active-site-bound spin probes in all human and rat MAOs remains similar in their respective detergent-purified and OMM-bound forms. Although these results cannot rule out the possibility of minor conformational alterations on purification in OGP micelles (as discussed above for hMAOA in Figure 2A and associated text), they do indicate that the overall structural properties of the active site cavities in human and rat MAOs do not differ significantly between their OMM-bound and OGP-purified forms.

Comparison of Spin Probe Accessibilities between MAOA and MAOB from Human and Rat. One of the most important observations made in this study is the relative differences in structural properties between the two MAO active site cavities from human and rat. Although the two human enzymes show nearly an order of magnitude difference in solvent accessibilities, the two rat enzymes show no difference (Table 3). This indicates that the active site cavities in MAOA and MAOB have evolved to adopt completely different architectures in the human lineage, whereas in rat they share similar structural properties. Although the physiological relevance of this drastic divergence between human and rat MAOs is not well understood, it does explain the origin of observed differences in inhibitors specificities between them, as reported earlier (*7*, *8*) and observed in this work with ParSL inhibitions (Table 1).

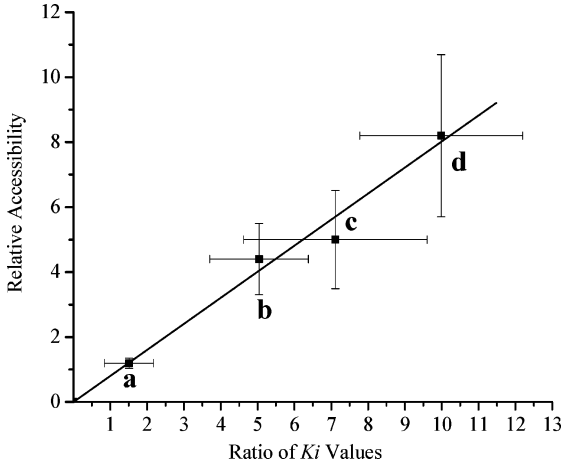

FIGURE 8: Correlation of the relative accessibilities of the active-site-bound spin probes in OMM-bound MAOs with the relative binding affinities of ParSL inhibition. The points (calculated from Tables 1 and 3) shown in the plot are as follows: a, $rMAOA_{OMM}$/$rMAOB_{OMM}$; b, $rMAOB_{OMM}$/$hMAOB_{OMM}$; c, $rMAOA_{OMM}$/$hMAOB_{OMM}$; d, $hMAOA_{OMM}$/$hMAOB_{OMM}$. The ratio of observed K_i values is related to the $\Delta(\Delta G)$ for the ParSL binding to the respective active sites.

The large difference observed in the spin probe accessibilities between the two human MAOs (Table 3) is consistent with the differences in their available X-ray structures and could be modeled by superimposing the ParSL spin probe into the clorgyline- and pargyline-inhibited structures of hMAOA and hMAOB (*1*, *3*), respectively (cf., Experiment Procedures). As indicated in Figure 7, the nitroxide-containing TEMPO ring of the ParSL spin probe (shown in blue) is exposed outside of the hMAOA active site cavity (Figure 7, inset), whereas in the hMAOB active site, the entire ParSL (shown in green) inhibitor remains buried inside the protein matrix (translucent gray surface in Figure 7). The differential orientations of the ParSL spin probes in hMAOA and hMAOB active sites are consistent with the orientations of the original inhibitors present in their crystal structures and reflect the differences in active site architectures of the two enzymes.

Correlation between Active Site Accessibilities and K_i's for ParSL Inhibitions. The differences in inhibitor specificities of ParSL between human and rat MAOs in their OMM-bound forms (Table 1) show a linear correlation with the differences in relative solvent accessibilities of their active-site-bound spin probes (Table 3). As shown in Figure 8, the two human MAOs with ca. 10-fold difference in accessibilities show an equivalent difference in their binding affinities (K_i values) of ParSL inhibition (data point d), whereas the two rat enzymes with comparable active site accessibilities show similar binding affinities of ParSL (data point a). Comparison of accessibilities and inhibitor specificities of the two rat MAOs with hMAOB also show similarly linear correlations (data points b and c, Figure 8). This indicates that the spin probe in a less solvent-accessible active site has a more favorable free energy of binding compared to a cavity with higher solvent accessibility. Thus, the ligand (ParSL) has more favorable protein interactions in an active site with low solvent accessibility than in one with a higher solvent accessibility. The correlation observed in Figure 8 demonstrates that the solvent accessibility of the spin probe (ParSL) directly correlates with the $\Delta(\Delta G)$ of its binding to the active sites. This is presumably a combined effect of hydrophobic and steric factors in MAO active sites. This correlation plot thus clearly indicates that the structural properties of the active site cavities in the two rat enzymes are distinctly different from those in the human enzymes and therefore serves as a basis in explaining the differences in their inhibitor specificities, as reported earlier (*7*, *8*).

Conclusions. In summary, using a spin-labeled inhibitor as an active-site-specific EPR spin probe, we have shown that the structural properties of the active site cavities in human and rat MAOs are different, which is responsible for the observed differences in their inhibitor specificities. Furthermore, the present data shows that the structural properties of MAOA and MAOB active site cavities are distinctly different in human, whereas in rat they are similar. Finally, the present data suggests that the overall structural properties of human and rat MAO active sites remain unaffected on purification in OGP micelles.

ACKNOWLEDGMENT

The authors thank Ms. Milagros Aldeco for providing the purified human MAOA and MAOB preparations used in this work. The authors also thank Dr. John Horton and Dr. Da Jia for their help in generating the ParSL superimposed structures of hMAOA and hMAOB.

REFERENCES

1. Binda, C., Newton-Vinson, P., Hubalek, F., Edmondson, D. E., and Mattevi, A. (2002) Structure of human monoamine oxidase B, a drug target for the treatment of neurological disorders, *Nat. Struct. Biol. 9*, 22−26.
2. Binda, C., Li, M., Hubalek, F., Restelli, N., Edmondson, D. E., and Mattevi, A. (2003) Insights into the mode of inhibition of human mitochondrial monoamine oxidase B from high-resolution crystal structures, *Proc. Natl. Acad. Sci. U.S.A. 100*, 9750−9755.
3. De Colibus, L., Li, M., Binda, C., Lustig, A., Edmondson, D. E., and Mattevi, A. (2005) Three-dimensional structure of human monoamine oxidase A (MAO A): Relation to the structures of rat MAO A and human MAO B, *Proc. Natl. Acad. Sci. U.S.A. 102*, 12684−12689.
4. Ma, J., Yoshimura, M., Yamashita, E., Nakagawa, A., Ito, A., and Tsukihara, T. (2004) Structure of rat monoamine oxidase A and its specific recognitions for substrates and inhibitors, *J. Mol. Biol. 338*, 103−114.
5. Mitoma, J., and Ito, A. (1992) Mitochondrial targeting signal of rat liver monoamine oxidase B is located at its carboxy terminus, *J. Biochem. 111*, 20−24.
6. Binda, C., Hubalek, F., Li, M., Edmondson, D. E., and Mattevi, A. (2004) Crystal structure of human monoamine oxidase B, a drug target enzyme monotopically inserted into the mitochondrial outer membrane, *FEBS Lett. 564*, 225−228.
7. Fierro, A., Osorio-Olivares, M., Cassels, B. K., Edmondson, D. E., Sepulveda-Boza, S., and Reyes-Parada, M. (2007) Human and rat monoamine oxidase-A are differentially inhibited by (*S*)-4-alkylthioamphetamine derivatives: Insights from molecular modeling studies, *Bioorg. Med. Chem. 15*, 5198−5206.
8. Novaroli, L., Daina, A., Favre, E., Bravo, J., Carotti, A., Leonetti, F., Catto, M., Carrupt, P.-A., and Reist, M. (2006) Impact of species-dependent differences on screening, design, and development of MAO B inhibitors, *J. Med. Chem. 49*, 6264−6272.
9. Fanucci, G. E., Lee, J. Y., and Cafiso, D. S. (2003) Membrane mimetic environments alter the conformation of the outer membrane protein BtuB, *J. Am. Chem. Soc. 125*, 13932−13933.
10. Fanucci, G. E., Lee, J. Y., and Cafiso, D. S. (2003) Spectroscopic evidence that osmolytes used in crystallization buffers inhibit a conformation change in a membrane protein, *Biochemistry 42*, 13106−13112.
11. Upadhyay, A. K., Borbat, P. P., Jin, W., Freed, J. H., and Edmondson, D. E. Determination of the oligomeric states of

human and rat monoamine oxidases in the outer mitochondrial membrane and octyl β-D-glucopyranoside micelles using pulsed dipolar electron spin resonance spectroscopy, *Biochemistry*, in press, 2007.
12. Kunji, E. R. S. (2004) The role and structure of mitochondrial carriers, *FEBS Lett. 564*, 239−244.
13. Kunji, E. R. S., and Harding, M. (2003) Projection structure of the atractyloside-inhibited mitochondrial ADP/ATP carrier of *Saccharomyces cerevisiae*, *J. Biol. Chem. 278*, 36985−36988.
14. Pebay-Peyroula, E., Dahout-Gonzalez, C., Kahn, R., Trezeguet, V., Lauquin, G. J. M., and Brandolin, G. (2003) Structure of mitochondrial ADP/ATP carrier in complex with carboxyatractyloside, *Nature 426*, 39−44.
15. Hubbell, W. L., Cafiso, D. S., and Altenbach, C. (2000) Identifying conformational changes with site-directed spin labeling, *Nat. Struct. Biol. 7*, 735−739.
16. Hubbell, W. L., Gross, A., Langen, R., and Lietzow, M. A. (1998) Recent advances in site-directed spin labeling of proteins, *Curr. Opin. Struct. Biol. 8*, 649−656.
17. Hubbell, W. L., and Altenbach, C. (1994) Investigation of structure and dynamics in membrane proteins using site-directed spin labeling, *Curr. Opin. Struct. Biol. 4*, 566−573.
18. Hubbell, W. L., McHaourab, H. S., Altenbach, C., and Lietzow, M. A. (1996) Watching proteins move using site-directed spin labeling, *Structure 4*, 779−783.
19. Merianos, H. J., Cadieux, N., Lin, C. H., Kadner, R. J., and Cafiso, D. S. (2000) Substrate-induced exposure of an energy-coupling motif of a membrane transporter, *Nat. Struct. Biol. 7*, 205−209.
20. Berliner, L. J. (1978) Spin labeling in enzymology: spin-labeled enzymes and proteins, *Methods Enzymol. 49*, 418−480.
21. Fanucci, G. E., and Cafiso, D. S. (2006) Recent advances and applications of site-directed spin labeling, *Curr. Opin. Struct. Biol. 16*, 644−653.
22. Columbus, L., and Hubbell, W. L. (2002) A new spin on protein dynamics, *Trends Biochem. Sci. 27*, 288−295.
23. Hubbell, W. L., and Altenbach, C. (1994) Site-directed spin labeling of membrane proteins, *Methods Physiol. Ser. 1*, 224−248.
24. Columbus, L., and Hubbell, W. L. (2004) Mapping backbone dynamics in solution with site-directed spin labeling: GCN4-58 bZip free and bound to DNA, *Biochemistry 43*, 7273−7287.
25. Liang, Z., Lou, Y., Freed, J. H., Columbus, L., and Hubbell, W. L. (2004) A multifrequency electron spin resonance study of T4 lysozyme dynamics using the slowly relaxing local structure model, *J. Phys. Chem. B 108*, 17649−17659.
26. Barnes, J. P., Liang, Z., McHaourab, H. S., Freed, J. H., and Hubbell, W. L. (1999) A multifrequency electron spin resonance study of T4 lysozyme dynamics, *Biophys. J. 76*, 3298−3306.
27. Watts, A. (1985) Spin-labels in biochemistry, *Biochem. Soc. Trans. 13*, 588−593.
28. Griffith, O. H., Dehlinger, P. J., and Van, S. P. (1974) Shape of the hydrophobic barrier of phospholipid bilayers (evidence for water penetration in biological membranes), *J. Membr. Biol. 15*, 159−192.
29. Zhang, J., Wallar, B. J., Popescu, C. V., Renner, D. B., Thomas, D. D., and Lipscomb, J. D. (2006) Methane monooxygenase hydroxylase and B component interactions, *Biochemistry 45*, 2913−2926.
30. Perozo, E., Kloda, A., Cortes, D. M., and Martinac, B. (2001) Site-directed spin-labeling analysis of reconstituted Mscl in the closed state, *J. Gen. Physiol. 118*, 193−205.
31. Altenbach, C., Froncisz, W., Hemker, R., McHaourab, H., and Hubbell, W. L. (2005) Accessibility of nitroxide side chains: Absolute Heisenberg exchange rates from power saturation EPR, *Biophys. J. 89*, 2103−2112.
32. Oh, K. J., Zhan, H., Cui, C., Altenbach, C., Hubbell, W. L., and Collier, R. J. (1999) Conformation of the diphtheria toxin T domain in membranes: A site-directed spin-labeling study of the TH8 helix and TL5 loop, *Biochemistry 38*, 10336−10343.
33. Cuello Luis, G., Cortes, D. M., and Perozo, E. (2004) Molecular architecture of the KvAP voltage-dependent K+ channel in a lipid bilayer, *Science 306*, 491−495.
34. Perozo, E., Cortes, D. M., Sompornpisut, P., Kloda, A., and Martinac, B. (2002) Open channel structure of MscL and the gating mechanism of mechanosensitive channels, *Nature 418*, 942−948.
35. Berliner, L. J., and McConnell, H. M. (1966) A spin-labeled substrate for a-chymotrypsin, *Proc. Natl. Acad. Sci. U.S.A. 55*, 708−712.
36. Wells, G. B., Mustafi, D., and Makinen, M. W. (1994) Structure at the active site of an acylenzyme of a-chymotrypsin and implications for the catalytic mechanism. An electron nuclear double resonance study, *J. Biol. Chem. 269*, 4577−4586.
37. Boisvert, W. E., Mustafi, D., Kasa, S., Makinen, M. W., Halpern, H. J., Yu, C., Barth, E., and Peric, M. (1993) Kinetically specific spin-label substrates of liver alcohol dehydrogenase and of liver aldehyde dehydrogenase, *Adv. Exp. Med. Biol. 328*, 501−512.
38. Buckman, T., and Eiduson, S. (1980) Studies of pargyline−monoamine oxidase binding using a spin label probe analog, *J. Neurochem. 34*, 1594−1602.
39. Huang, R. H., and Eiduson, S. (1977) Significance of multiple forms of brain monoamine oxidase in situ as probed by electron spin resonance, *J. Biol. Chem. 252*, 284−290.
40. Huang, R. H., Eiduson, S., and Shih, J. C. (1976) Determination of monoamine oxidase in rat brain by electron spin resonance techniques, *J. Neurochem. 26*, 799−803.
41. Altenbach, C., Greenhalgh, D. A., Khorana, H. G., and Hubbell, W. L. (1994) A collision gradient method to determine the immersion depth of nitroxides in lipid bilayers: application to spin-labeled mutants of bacteriorhodopsin, *Proc. Natl. Acad. Sci. U.S.A. 91*, 1667−1671.
42. Cuello Luis, G., Cortes, D. M., and Perozo, E. (2004) Molecular architecture of the KvAP voltage-dependent K+ channel in a lipid bilayer, *Science 306*, 491−495.
43. Alonso, A., Pereira Dos Santos, W., Leonor, S. J., Goncalves Dos Santos, J., and Tabak, M. (2001) Stratum corneum protein dynamics as evaluated by a spin-label maleimide derivative: effect of urea, *Biophys. J. 81*, 3566−3576.
44. Rando, R. R. (1977) The fluorescent labeling of mitochondrial monoamine oxidase, *Mol. Pharmacol. 13*, 726−734.
45. Newton-Vinson, P., Hubalek, F., and Edmondson, D. E. (2000) High-level expression of human liver monoamine oxidase B in *Pichia pastoris*, *Protein Expression Purif. 20*, 334−345.
46. Li, M., Hubalek, F., Newton-Vinson, P., and Edmondson, D. E. (2002) High-level expression of human liver monoamine oxidase A in *Pichia pastoris*: comparison with the enzyme expressed in *Saccharomyces cerevisiae*, *Protein Expression Purif. 24*, 152−162.
47. Hubalek, F., Binda, C., Khalil, A., Li, M., Mattevi, A., Castagnoli, N., and Edmondson, D. E. (2005) Demonstration of isoleucine 199 as a structural determinant for the selective inhibition of human monoamine oxidase B by specific reversible inhibitors, *J. Biol. Chem. 280*, 15761−15766.
48. Daum, G., Boehni, P. C., and Schatz, G. (1982) Import of proteins into mitochondria. Cytochrome *b*2 and cytochrome *c* peroxidase are located in the intermembrane space of yeast mitochondria, *J. Biol. Chem. 257*, 13028−13033.
49. Walker, M. C., and Edmondson, D. E. (1994) Structure−activity relationships in the oxidation of benzylamine analogues by bovine liver mitochondrial monoamine oxidase B, *Biochemistry 33*, 7088−7098.
50. Murib, J. H., and Ritter, D. M. (1952) Decomposition of nitrosyldisulfonate ion. I. Products and mechanism of color fading in acid solution, *J. Am. Chem. Soc. 74*, 3394−3398.
51. Farahbakhsh, Z. T., Altenbach, C., and Hubbell, W. L. (1992) Spin labeled cysteines as sensors for protein−lipid interaction and conformation in rhodopsin, *Photochem. Photobiol. 56*, 1019−1033.
52. Kirby, T. L., Karim, C. B., and Thomas, D. D. (2004) Electron paramagnetic resonance reveals a large-scale conformational change in the cytoplasmic domain of phospholamban upon binding to the sarcoplasmic reticulum Ca-ATPase, *Biochemistry 43*, 5842−5852.
53. Jones, T. A., Zou, J. Y., Cowan, S. W., and Kjeldgaard, M. (1991) Improved methods for building protein models in electron density maps and the location of errors in these models, *Acta. Crystallogr., Sect. A 47 (Pt 2)*, 110−119.
54. Saxl, R. L., Reston, J., Nie, Z., Kalman, T. I., and Maley, F. (2003) Modification of *Escherichia coli* thymidylate synthase at tyrosine-94 by 5-imidazolylpropynyl-2′-deoxyuridine 5′-monophosphate, *Biochemistry 42*, 4544−4551.
55. Kitz, R., and Wilson, I. B. (1962) Esters of methanesulfonic acid as irreversible inhibitors of acetylcholinesterase, *J. Biol. Chem. 237*, 3245−3249.
56. McHaourab, H. S., Lietzow, M. A., Hideg, K., and Hubbell, W. L. (1996) Motion of spin-labeled side chains in T4 lysozyme.

Correlation with protein structure and dynamics, *Biochemistry 35*, 7692−7704.
57. Hilger, D., Jung, H., Padan, E., Wegener, C., Vogel, K.-P., Steinhoff, H.-J., and Jeschke, G. (2005) Assessing oligomerization of membrane proteins by four-pulse DEER: pH-dependent dimerization of NhaA Na+/H+ antiporter of *E. coli*, *Biophys. J. 89*, 1328−1338.
58. Hubalek, F., Pohl, J., and Edmondson, D. E. (2003) Structural comparison of human monoamine oxidases A and B: mass spectrometry monitoring of cysteine reactivities, *J. Biol. Chem. 278*, 28612−28618.
59. Krueger-Koplin, R. D., Sorgen, P. L., Krueger-Koplin, S. T., Rivera-Torres, I. O., Cahill, S. M., Hicks, D. B., Grinius, L., Krulwich, T. A., and Girvin, M. E. (2004) An evaluation of detergents for NMR structural studies of membrane proteins, *J. Biomol. NMR 28*, 43−57.

BI7019707